RSC Advances

ROYAL SOCIETY OF CHEMISTRY

www.rsc.org/advances

Highly selective and sensitive colorimetric chemosensors for Hg^{2+} based on novel diaminomaleonitrile derivatives

Yanping Huo [a, b,*], Songying Wang [a], Tianhua Lu [a], Chengqiang Pan [a], Yujing Lu [a], Xianghua Yang [a], Dongping Hu [a], Sheng Hu [a]

[a] *School of Chemical Engineering and Light Industry, Guangdong University of Technology, Guangzhou 510006, China*

[b] *Key laboratory of Organofluorine Chemistry, Shanghai Institute of Organic Chemistry, Chinese Academy of Sciences, Shanghai 200032, China*

*Corresponding authors. Tel.: +86 20 39322236; Fax: +86 20 39322235 Mobile: +86 13798135622.

E-mail addresses: yphuo@gdut.edu.cn (Y. Huo)

ABSTRACT

Five novel soluble chemosensors in $EtOH/H_2O$ based on schiff-base diaminomaleonitrile derivatives which were modified by different aromatic functional moieties have been synthesized. These chemosensors were fully characterized by ^1H NMR, ^{13}C NMR spectroscopy, mass spectrometry, and single crystal X-ray diffraction. The recognition abilities of these chemosensors with a range of metal ions at different pH values were evaluated and their photophysical properties have been systematically investigated. DFT theoretical calculations were employed to understand the behaviors of the chemosensors toward Hg^{2+}. The sensing mechanism was derived through experimental and theoretical calculations. All the results

consistently indicated that these diaminomaleonitrile derivatives were ideal chemosensors for the detection of Hg^{2+} in aqueous solutions.

Keywords

Diaminomaleonitrile derivatives; Colorimetric chemosensors; Aromatic group modifying; Hg^{2+} detection; DFT theoretical calculations

Introduction

In the past decades, many metals and their alloys have been widely used in industrial, military, civil and other fields. However, some heavy metal ions and transition metal ions are harmful to the environment. In particular, Hg^{2+} ion is regarded as one of the most toxic metal ions. Accumulation of Hg^{2+} over time in the bodies of humans and animals can lead to serious debilitating illnesses and central nervous system damages.[1,2] Therefore, the development of increasingly selective and sensitive methods for the detection of Hg^{2+} is currently receiving considerable attention.[3–7] Current detection methods for Hg^{2+} ion use atomic absorption spectrometry and inductively coupled plasma-mass spectrometry and share some drawbacks of needing expensive instruments and time-consuming procedures.[8] Colorimetric chemosensors for Hg^{2+} ion have attracted considerable attention due to their simple naked eye detection, inexpensive instrumentation, and its potential environmental applications.[9–15] Consequently, a broad range of colorimetric chemosensors for Hg^{2+} ion have been reported.[9–15] However, it is highly challenging to synthesize new

reversible colorimetric chemosensors for Hg^{2+} ion with ideal water solubility, excellent selectivity and outstanding sensitivity.[16]

In recent years, many researchers reported diaminomaleonitrile (DMN) derivatives[17–19] as fluorescent probes for Hg^{2+} ion detection in ethanol–water solution with their high detection abilities. Our synthetic strategy was to create an extensive donor–acceptor system by incorporating electron donor (aromatic) and a strong electron acceptor (diaminomaleonitrile) within the same framework. The extended π-conjugation enhanced the intramolecular charge transfer (ICT), which is expected to be highly sensitive towards external perturbations such as metal ion proximity resulting into optical and spectral changes.[20–22] The diaminomaleonitrile was chosen not only for its ability to act as diamine and form simple schiff-base ligands but also for the fact that the electron-withdrawing CN groups, which clearly affect the coordinating capacity of DMN itself.[23] In addition, an imine group, which was easily dissolved in aqueous solution was brought in to improve the solubility of the chemosensors and enlarge their extent of applications, concurrently modulate the coordinating properties of molecules cooperatively with DMN.[24] Inspired by this idea, we have synthesized a series of chemosensors by coupling diaminomaleonitrile with different functionalized aromatic aldehydes (scheme 1). These organic ligands displayed dramatic color change with Hg^{2+} in aqueous solutions at room

temperature immediately.

Experimental

Materials and instruments

1-Pyrenecarboxaldehyde was purchased from TCI (Shanghai) Development Company. 4-Fluorobenzaldehyde, 4-tert-butylbenzaldehyde, 2,3,4-trimethoxybenzaldehyde and diaminomaleonitrile were purchased from J&K Chemial. EtOH was spectrometric grade. Metal salts $LiNO_3$, $NaNO_3$, KNO_3, $Mg(NO_3)_2$, $Ca(NO_3)_2$, $Ba(NO_3)_2$, $Cu(NO_3)_2$, $Zn(NO_3)_2$, $Co(NO_3)_2$, $Ni(NO_3)_2$, $Cd(NO_3)_2$, $AgNO_3$, $Hg(NO_3)_2$, $Pd(NO_3)_2$, $Fe(NO_3)_3 \cdot 9H_2O$, $Cr(NO_3)_3$ were purchased from Aldrich.

All of the chemicals were commercially available, and used without further purification. Elemental analyses were performed with an EA1110 CHNS-0 CE elemental analyzer. Absorbance spectra were collected by a Perkin Elmer Lambda 25 UV–vis spectrophotometer using quartz cells of 1.0 cm path length. ^{1}H, ^{19}F and ^{13}C NMR experiments were carried out on a MERCURY plus 400 spectrometer operating at resonance frequencies of 100.63 MHz. Electrospray ionization mass spectra (ESI-MS) were recorded on a Finnigan LCQ mass spectrometer using dichloromethane/methanol as mobile phase. All electron DFT calculations were performed using a Dmol3 package in Gaussian 09W.

Synthesis

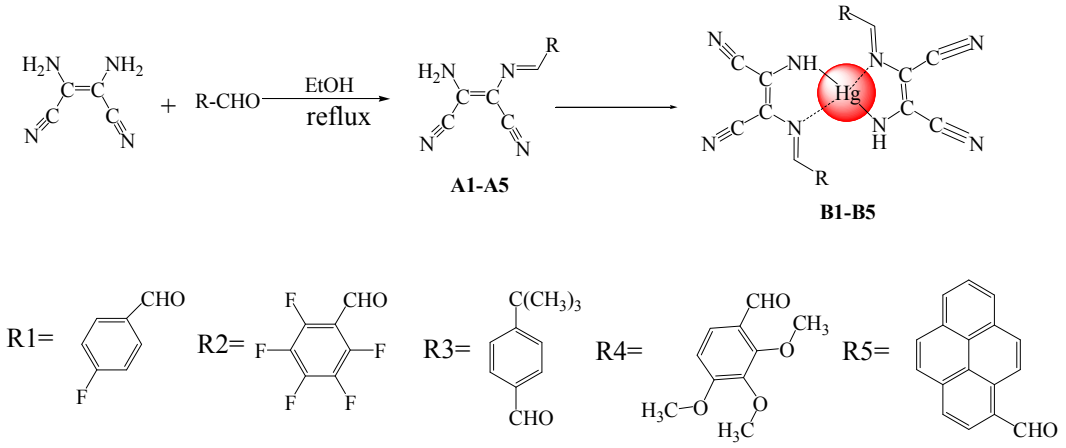

Scheme 1. Syntheses of ligands **A1**–**A5**.

Preparation of N-(4-fluorobenzyl)-2-aminomalonitrile (A1)

To a solution of 4-fluorobenzaldehyde (0.57 g, 4.6 mmol) in ethanol (20 mL) was added diaminomaleonitrile (0.50 g, 4.6 mmol) dissolved. The mixture was heated under reflux for 8 h. The yellow precipitate obtained was filtered off, washed with ethanol 3 times and water 3 times, and dried overnight with oven. Yield = 0.94 g, 87%. ^{1}H NMR (400 MHz, DMSO) δ 8.30–7.82 (m, 5H), 7.40–7.21 (m, 2H). ^{19}F NMR (376 MHz, DMSO) δ -108.25 (s). ^{13}C NMR (101 MHz, DMSO) δ 165.77, 163.28, 154.22, 131.81, 127.46, 116.06, 114.85, 114.21, 102.92, 97.22, 54.95. EI-MS: *m*/*z* calcd for 214 $(M + 1)^{+}$, found 214. Element analysis (%): Anal. Calc. for $C_{11}H_7FN_4$: C, 61.68; H, 3.29; F, 8.87; N, 26.16. Found: C, 61.59; H, 3.51; F, 8.76; N, 26.14.

Preparation of N-(pentafluorobenzyl)-2-aminomalonitrile (A2)

To a solution of pentafluorobenzaldehyde (0.90 g, 4.6 mmol) in ethanol (20 mL) was added diaminomaleonitrile (0.50 g, 4.6 mmol) dissolved. The

mixture was heated under reflux for 8 h. The yellow precipitate obtained was filtered off, washed with ethanol 3 times and water 3 times, and dried overnight with oven. Yield = 1.07 g, 76%. ^{1}H NMR (400 MHz, DMSO) δ 8.50 (s, 1H), 8.12 (d, J = 37.4 Hz, 2H). ^{19}F NMR (376 MHz, DMSO) δ -141.50 (s), -142.96 (s), -151.47 (s), -162.63 (s), -162.78 (s). EI-MS: *m*/*z* calcd for 286 $(M + 1)^{+}$, found 286. Element analysis (%): Anal. Calc. for $C_{11}H_3F_5N_4$: C, 46.17; H, 1.06; F, 33.20; N, 19.58. Found: C, 46.09; H, 1.37; F, 33.02; N, 19.52.

Preparation of N-(4-tert-butylbenzyl)-2-aminomalonitrile (A3)

To a solution of 4-tert-butylbenzaldehyde (1.08 g, 4.6 mmol) in ethanol (20 mL) was added diaminomaleonitrile (0.50 g, 4.6 mmol) dissolved. The mixture was heated under reflux for 10 h. The yellow precipitate obtained was filtered off, washed with ethanol 3 times and water 3 times, and dried overnight with oven. Yield = 0.83 g, 87%. ^{1}H NMR (400 MHz, $CDCl_3$) δ 8.40 (s, 1H), 7.75 (d, J = 7.6 Hz, 2H), 7.48 (d, J = 7.7 Hz, 2H), 5.25 (s, 2H), 1.34 (s, 9H). EI-MS: *m*/*z* calcd for 252.10 $(M + 1)^{+}$, found 252.95. Element analysis (%): Anal. Calc. for $C_{15}H_{16}N_4$: C, 71.40; H, 6.39; N, 22.21. Found: C, 71.48; H, 6.45; N, 22.17.

Preparation of N-(2,3,4-trimethoxybenzyl)-2-aminomalonitrile(A4)

To a solution of 2,3,4-trimethoxybenzaldehyde (0.91 g, 4.6 mmol) in ethanol (20 mL) was added diaminomaleonitrile (0.50 g, 4.6 mmol)

dissolved. The mixture was heated under reflux for 14 h. The yellow precipitate obtained was filtered off, washed with ethanol 3 times and water 3 times, and dried overnight with oven. Yield = 1.03 g, 73%. ^{1}H NMR (400 MHz, $CDCl_3$) δ 8.70 (s, 1H), 7.72 (d, J = 8.3 Hz, 1H), 7.26 (s, 1H), 6.72 (d, J = 9.3 Hz, 1H), 5.11 (s, 2H), 4.01–3.83 (m, 9H). ^{13}C NMR (101 MHz, DMSO) δ 157.19, 154.34, 150.81, 141.91, 126.24, 123.39, 121.63, 114.88, 114.18, 108.81, 103.81, 62.19, 61.19, 56.89. EI-MS: *m*/*z* calcd for 286.1 $(M + 1)^+$, found 286.9. Element analysis (%): Anal. Calc. for $C_{14}H_{14}N_4O_3$: C, 58.73; H, 4.93; N, 19.57; O, 16.77. Found: C, 58.60; H, 5.09; N, 19.51; O, 16.80.

Preparation of N-(pyrenyl)-2-aminomalonitrile (A5)

To a solution of 1-pyrenecarboxaldehyde (1.06 g, 4.6 mmol) in ethanol (20 mL) was added diaminomaleonitrile (0.50 g, 4.6 mmol) dissolved. The mixture was heated under reflux for 10 h. The yellow precipitate obtained was filtered off, washed with ethanol 3 times and water 3 times, and dried overnight with oven. Yield = 0.94 g, 63.5%. ^{1}H NMR (400 MHz, $CDCl_3$) δ 9.39–9.22 (s, 1H), 9.01–8.92 (s, 1H), 8.80–8.66 (s, 1H), 8.45–7.94 (m, 9H). ^{13}C NMR (101 MHz, DMSO) δ 152.52, 133.44, 131.30, 130.46, 130.24, 129.57, 127.91, 127.72, 127.25, 127.06, 126.88, 126.66, 125.47, 124.38, 124.10, 122.07, 115.08, 114.30, 104.28, 97.22, 54.95, 49.08. EI-MS: *m*/*z* calcd for 321 $(M + 1)^+$, found 321. Element analysis (%): Anal. Calc. for $C_{21}H_{12}N_4$: C, 78.73; H, 3.78; N, 17.49. Found: C, 78.69; H, 3.86; N, 17.45.

Preparation of [Hg(A4)$_2$] (B4)

A mixture of $Hg(NO_3)_2$, (0.08 mmol, 25.96 mg), **A4** (0.04 mmol, 11.48 mg), H_2O (0.2 mL), DMF (0.2 mL) and EtOH (2 mL) in a capped vial was heated at 80 °C for one day. Yellow block like crystals of **B4** suitable for single-crystal X-ray diffraction were collected, washed with ether and dried in air. Yield = 12.61 mg, 82%. Element analysis (%): Anal. Calc. for $C_{28}H_{24}N_8O_6Hg$: C, 43.69; H, 3.12; N, 14.56. Found: C, 43.71; H, 3.10; N, 14.57.

Results and discussions

Colorimetric study

Colorimetric sensing by naked eye is the simplest way to observe the selectivity of chemosensor to various metal cations. As shown in Fig. 1, under daylight lamp irradiation, upon the addition of 1.0 equiv. of K^+, Ca^{2+}, Ba^{2+}, Co^{2+}, Cd^{2+}, Mg^{2+}, Ag^+, Na^+, Fe^{3+}, Hg^{2+}, Cu^{2+}, Ni^{2+}, Al^{3+}, Zn^{2+}, Cr^{3+} and Pd^{2+} metal ions, chemosensors **A1–A5** displayed a dramatic color change with Hg^{2+} in EtOH/H_2O at room temperature immediately, whereas no significant changes were found with other tested metal cations. The selective color change can be used for the "naked eye" detection of Hg^{2+} in aqueous solutions.[25]

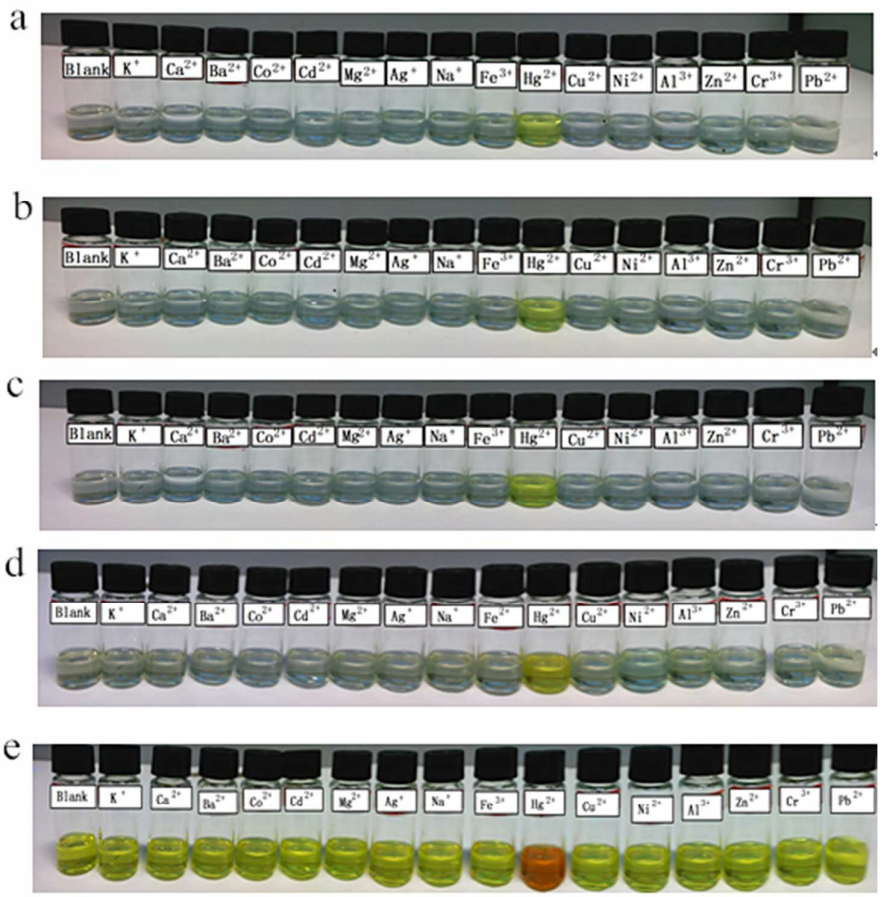

Fig. 1. Solutions of five chemosensors upon addition of different metal ions in EtOH/H_2O (v/v = 4:1,). The color changed of (a), (b), (c), (d), (e) is the diagram of **A1**, **A2**, **A3**, **A4** and **A5**, respectively. [**A1–A5**] =40 μM, [M^{n+}] = 200 μM.

UV-vis spectrophotometric estimation of Hg^{2+} binding with A1–A5

The UV-vis spectra of the chemosensors **A1–A5** in EtOH/H_2O (v/v = 4:1, 1.0×10^{-5} M) solutions were characterized by two bands. The strong absorption peaks centered (max) at 362, 364, 365, 377 and 421 nm, respectively. The band centered at about 250 to 300 nm can be tentatively assigned to a charge-transfer band from donor to acceptor, corresponding to the π–π* absorbance of diaminomaleonitrile.[26,27] For the chemosensors

based on ICT, electron-donating functional groups can greatly enhance the electron-donating ability of electron donors and result in a red-shift in the absorption spectra. As shown in Fig. 2, due to the conjugation pyrene ring, **A5** has the largest red-shift amongst the five chemosensors. This phenomenon can be ascribed to the varied electron-donating ability of the donators. The trimethoxybenzyl group also has an effect on D-π-A conjugate system causing about a decade nanometers red-shifted in **A1**–**A3**. Fluorobenzyl group and pentafluorobenzyl group are electron-withdrawing groups which make the π–π* absorbance of **A1** and **A2** blue-shifted to shorter wavelength.

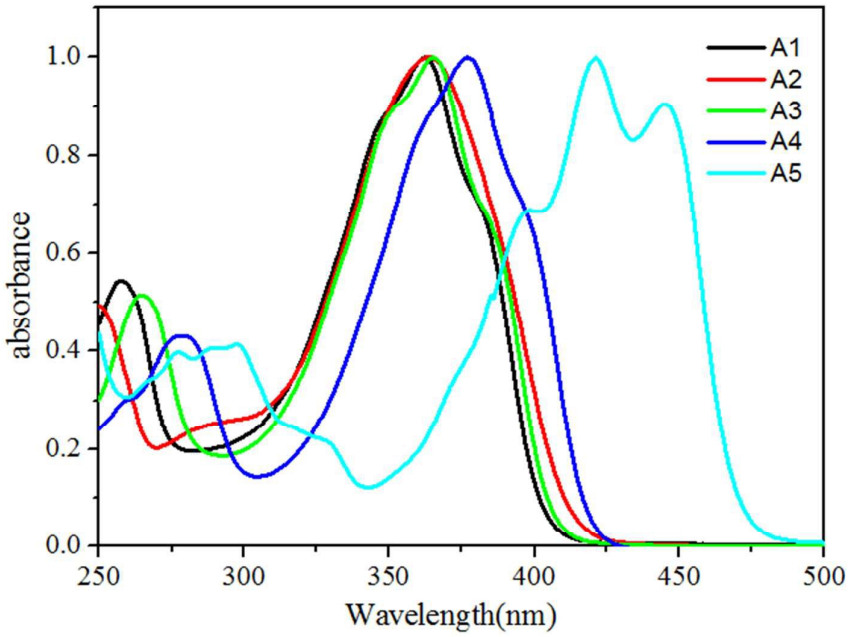

Fig. 2. Changes in absorption spectra of **A1**–**A5** by alternating irradiation with UV-vis in EtOH/H_2O (v/v = 4:1, 1.0×10^{-5} M) at room temperature.

The ability of chemosensor **A4** to form complex with metal ions was

also studied using UV-vis spectroscopy (Fig. 3). The addition of Hg^{2+} to **A4** caused a 28 nm red-shifted (from 377 to 405 nm), which changed the color from grey to yellow (Fig. 1). This phenomenon is similar to the addition of Hg^{2+} to chemosensors **A1**, **A2**, **A3** and **A5**, respectively (Fig. S16, Fig. S17, Fig. S18 and Fig. S19, in the Electronic Supplementary Information). Hg^{2+} ion binding with chemosensors **A1–A5** caused identical red-shifts and color changes. Hg^{2+} ion can induce deprotonation of active NH groups, especially those conjugated to aromatic or carbonyl groups. Such deprotonation process caused by complexation can be used for metal ions recognition and sensing.[28] For the chemosensors based on ICT, the deprotonation of those coordinated atoms in electron-donating groups can greatly enhance their electron-donating ability and result in a red-shifted in absorption spectra. These results indicate the occurrence of coordination between the five chemosensors and Hg^{2+}.

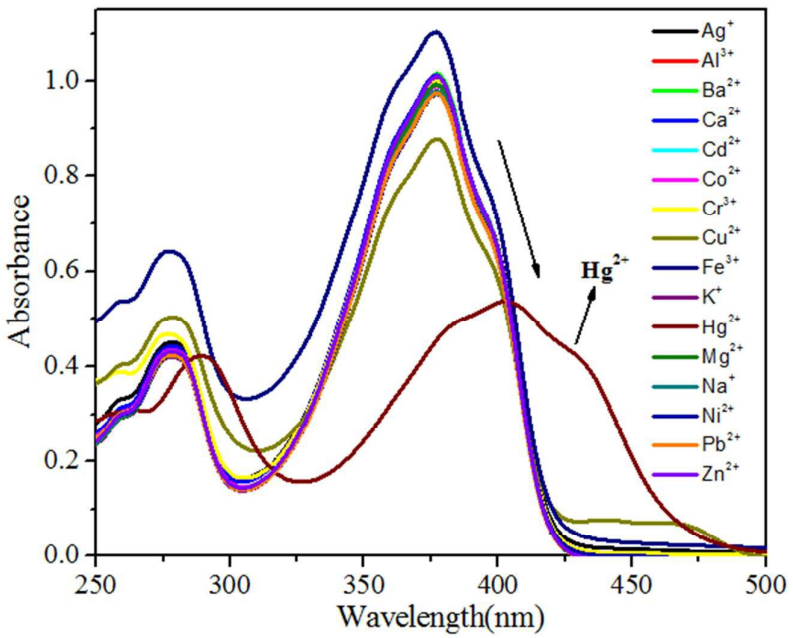

Fig. 3. Absorption changes of **A4** in EtOH/H_2O (v/v = 4:1, 1.0×10^{-5} M) upon addition of 1 equiv of different nitrate salts(1.0×10^{-5} M).

To study the influence of other metal ions (Ag^+, Al^{3+}, Ba^{2+}, Ca^{2+}, Cd^{2+}, Co^{2+}, Cr^{3+}, Cu^{2+}, Fe^{3+}, K^+, Mg^{2+}, Na^+, Ni^{2+}, Pb^{2+} and Zn^{2+}) on Hg^{2+} the binding of with **A1**–**A5**, competitive absorption spectroscopic were experiments performed with Hg^{2+} (1.0×10^{-5} M) in the presence of other metal ions (5.0×10^{-5} M). Take **A4** for example (Fig. 4.), bars represent for the absorbance at the biggest intensity band of chemosensers. Green bars represent the addition of 2 equivalent of metal ions (Ag^+, Al^{3+}, Ba^{2+}, Ca^{2+}, Cd^{2+}, Co^{2+}, Cr^{3+}, Cu^{2+}, Fe^{3+}, K^+, Mg^{2+}, Na^+, Ni^{2+}, Pb^{2+}, Zn^{2+} and blank, respectively) to the chemosensor solution. Red bars represent the subsequent addition of 1 equivalent of Hg^{2+} to the solution in the presence of competitive cations. Absorption changes caused by the mixture of Hg^{2+} with other metal ions were similar to that of Hg^{2+} alone. These facts

confirmed that the selectivity of **A1–A5** for Hg^{2+} ion detection is higher than other metal ions.

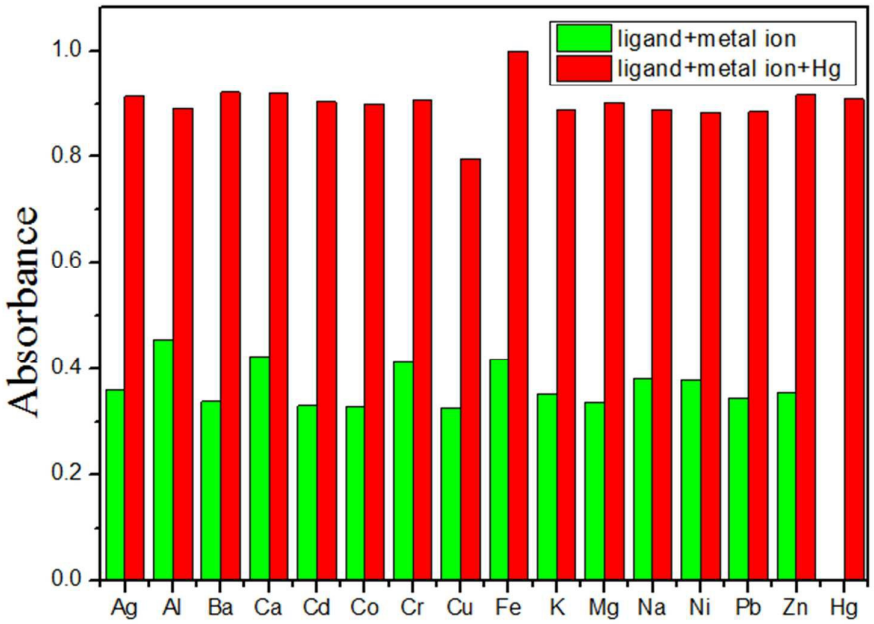

Fig. 4. Absorbance of **A4**-Hg^{2+} at the new band upon addition of various cations. The low bars represent **A4** (1.0×10^{-5} M) with cations (5.0×10^{-5} M) without Hg^{2+}; the high bars represent **A4** (1.0×10^{-5} M) with cations (5.0×10^{-5} M) upon the subsequent addition of Hg^{2+} (1.0×10^{-5} M) in EtOH/H_2O(v/v = 4:1).

Detection limits and association constants

In order to prove the selectivity of **A1–A5** towards Hg^{2+}, the detection limits[29] were calculated as shown in table 1. Assuming a 2 : 1 molar ratio forms the ligand/Hg^{2+} complex, the association constant (K) was calculated on the basis of the titration curves of **A1–A5** with Hg^{2+}. To further confirm the superior selectivities of **A1–A5** towards Hg^{2+}, the pH effects of their responses are evaluated as explained below.

Table 1
Calculated stability constant and detection limit data for **A1–A5**.

	k	Detection limit

A1	6.88×10^{2}	2.40×10^{-6}
A2	4.89×10^{2}	3.13×10^{-6}
A3	3.11×10^{3}	2.74×10^{-6}
A4	3.62×10^{3}	1.93×10^{-6}
A5	2.12×10^{3}	3.13×10^{-6}

Stoichiometries and affinity constants of chemosensors with Hg^{2+}

To explore the quantitative interrelation and the interaction mode of chemosensors with Hg^{2+} ion, the coordination reaction of **A4** with Hg^{2+} ion was monitored by UV–vis spectroscopic titration (Fig. 5). After the addition of Hg^{2+} ion (0.5 equimolar per drop), the peak of **A4** at 279 nm showed significant red-shifted (about 9 nm) to the peak of **B4** at 288 nm. The peak at 377 nm was found to become weaker and red-shifted with increasing amounts of Hg^{2+} ion. A new band centered at 382 nm started to develop with a distinct isosbestic point at 405 nm, indicating strong interactions between **A4** and the Hg^{2+}. No difference was observed in the absorption spectra once the 2:1 molar ratio of **A4**/Hg^{2+} was reached, which clearly indicated the formation of $[Hg(\mathbf{A4})_2]_n$.

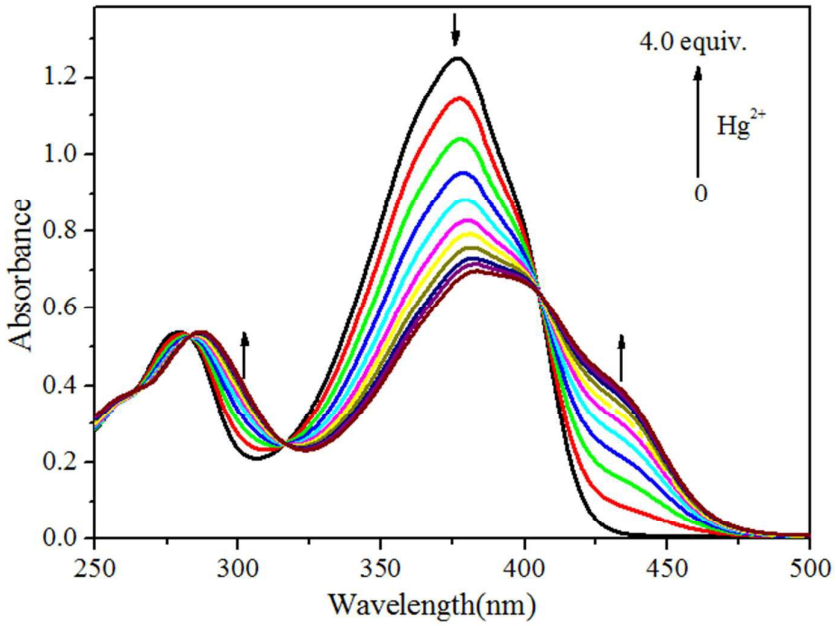

Fig. 5. UV–vis titration curves of **A4** in EtOH/H_2O in the presence of different amounts of Hg^{2+}.

In order to further ensure the binding sites of **A1**–**A5**, take **A4** for example, the stoichiometries of **A4** + Hg^{2+} were calculated through Job's plots as shown in Fig. 6 the stoichiometries of **A4** + Hg^{2+} was established by Job's plots between the mole fraction (X_M) and maximum absorption intensities at 430 nm, respectively. Upon the addition of 0–30 μM of Hg^{2+} (with an equal span of 3 μM), the absorption maxima of **A4** were quenched rapidly up to 10 μM, afterwards they were found to be restored again. Therefore, the Job's plots intensities displayed a absorption maxima at a molar fraction of ca. 0.66 (**A4** + Hg^{2+}), as shown in Fig. 6, representing their 2:1 stoichiometric complexation.[30]

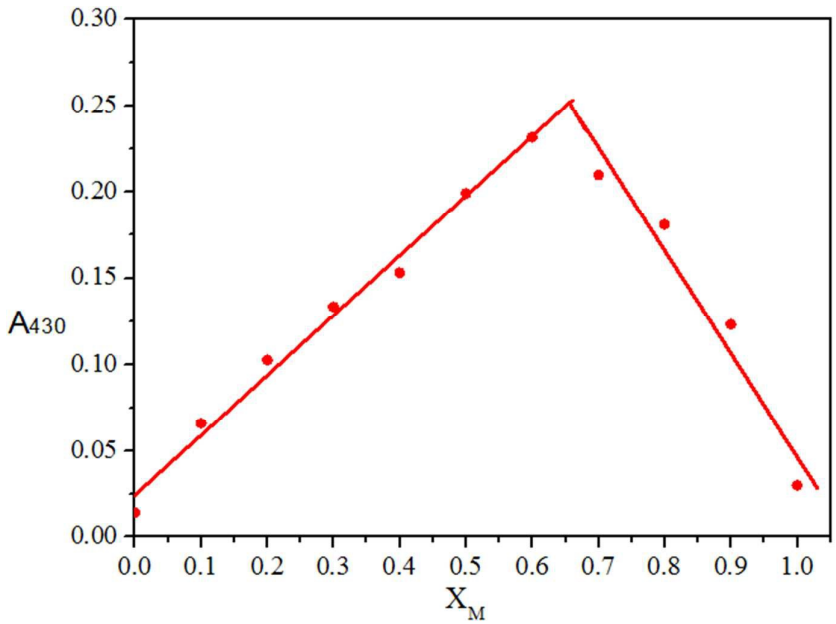

Fig. 6. Absorbance spectral changes of stoichiometry calculations based on absorbance intensities at 430 nm; $X_M = [Hg^{2+}]/([Hg^{2+}] + [\mathbf{A4}])$; where X_M = mole fraction, $[Hg^{2+}]$ and [**A4**] are concentrations of Hg^{2+} and **A4**; **A4** + Hg^{2+} = 2:1 stoichiometry (ca. 0.66).

Benesi-Hildebrand (B-H) method is a widely used approach in physical chemistry for the determination of equilibrium constant *K* and stoichiometry of non-bonding interactions. This approach could generate stoichiometric conclusions for bonding interaction, such as charge-transfer complexes and host-guest molecular complexation.

$$nL + M \longrightarrow ML_n$$

$$\frac{1}{A - A_\circ} = \frac{1}{K(A_l - A_\circ)[M]^n} + \frac{1}{A_l - A_\circ}$$

According to Benesi-Hildebrand equation

Taking logarithm on both side of equation

$$\lg\frac{(A_l - A_\circ)}{(A - A_\circ)} = -\lg K + n\lg\frac{1}{[M]}$$

Here in: A_1 is the absorbance of Hg^{2+} ion solution balanced. A_0 is the absorbance of Hg^{2+} ion absent solution. $[Hg^{2+}]$ is the concentration of Hg^{2+} ion, K is the stability constant, and n is the stoichiometry of ligand and metal ion.

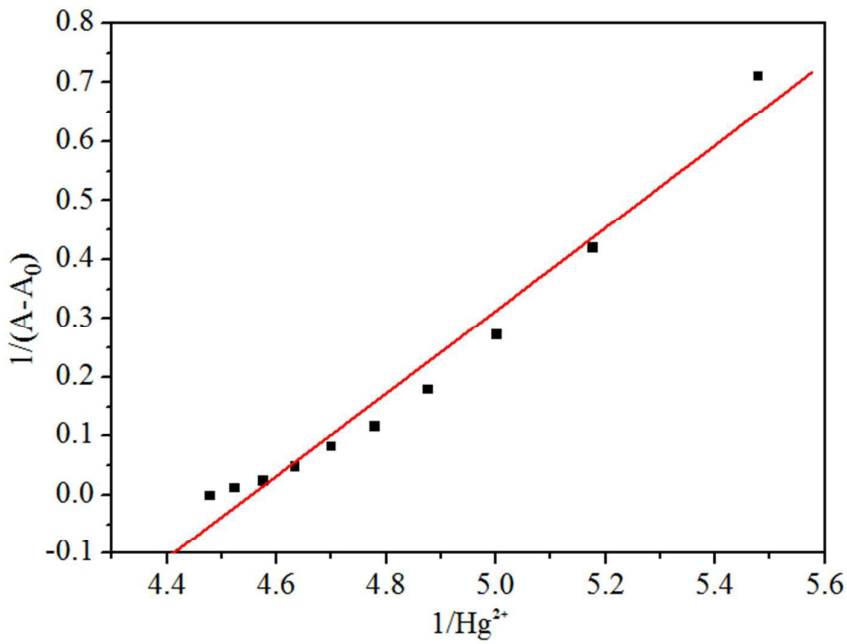

Fig. 7. Benesi-Hildebrand plot of the Hg^{2+}-**A4** complexes in EtOH/H_2O solution

Based on the 2:1 stoichiometry and the Job's plot, the stability constant of the complex between **A1** and Hg^{2+} was estimated to be 6.88×10^2 by plotting $\lg[(A_l–A_0)/(A–A_0)]$ against $\lg\{1/[Hg^{2+}]\}$, all the experiment-based stability constants are calculated listed in Table 1. From table 1, **A3** has the biggest stability constant of the five chemosensors, meaning **A3** has the greatest potential application as Hg^{2+} chemosensor. Due to its wide absorbance peak and poor red-shift ability, **A5** does not perform as well as the other four ligands.

pH effects

To demonstrate the Hg^{2+}-induced deprotonation of the imine group in **A1–A5**, pH titration experiments were carried out. First, the influence of pH on chemosensor **A4** was studied using UV-vis spectroscopy. Over a pH range of 5–10, the visible absorption band centered at 405 nm stays unchanged. A decrease in pH from 5 to 1 engendered a shift in the maximum absorption wavelength, which was due to protonation of the imine group.[16] The effect of pH on Hg^{2+} binding to **A4** was further studied by monitoring **A4**-Hg^{2+} complex at a wavelength of 405 nm (Fig. 8). The absorbance suddenly increased at pH 5.0 and reached a maximum over a pH range of 5.0–10.0, indicating that the formation of **A4**-Hg^{2+} complex is a deprotonation process.[31] When the pH value exceeded 10, the absorbance gradually decreased duing to the dissociation of **A4**-Hg^{2+} complex, which resulted in lower absorbance at 405 nm. The absorbance was almost negligible at pH values less than 3 clearly that evidently the **A4**-Hg^{2+} complex do not exist over this pH range.[32] Because the five chemosensors were modified by different electron functional aromatic moieties, their abilities of protonation and deprotonation were different. Therefore, the five chemosensors' detection ranges of pH values were different.

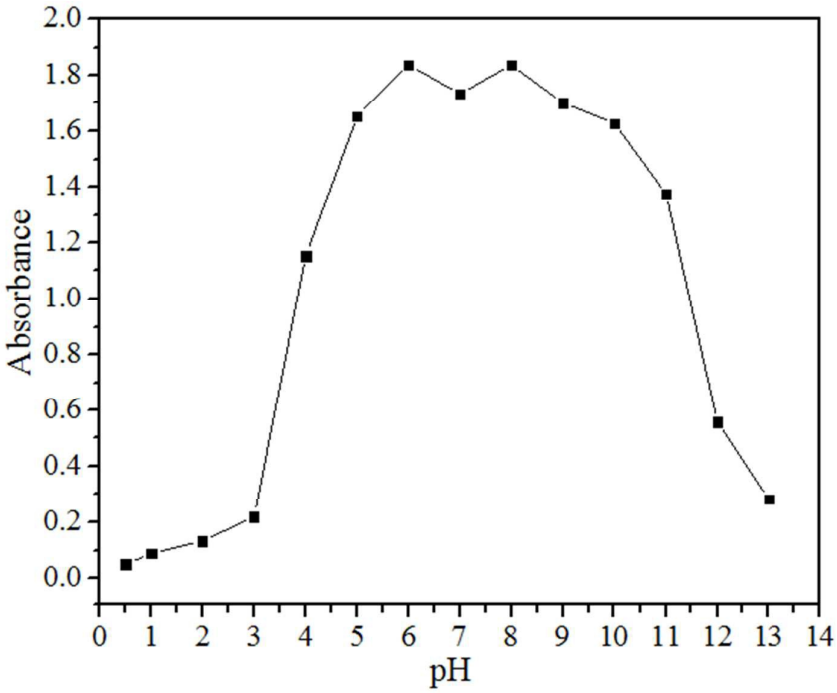

Fig. 8. The stable range of pH values on **A4**, chemosensor **A4** (1.0×10^{-5} M) was added in 1.0 mL EtOH/H_2O solution (v/v = 4:1, 20 mM buffer). The buffers were: pH 1.0–2.0, HCl; pH 2.5–4.0, KHP/HCl; pH 4.5–6.0, KHP/NaOH; pH 6.5–10.0 Hepes/NaOH, pH 11.0–12.0 NaOH.

single crystal diffraction study

Table 2.

Crystal data and structure refinement for **A4** and **B4**

Identification code	**A4**	**B4**
Empirical formula	$C_{14}H_{14}N_4O_3$	$C_{28}H_{24}HgN_8O_6$
M_r /g mol^{-1}	286.29	769.14
T /K	110(2)	153(2)
Crystal system	monoclinic	monoclinic
Space group	$P2_1/c$	$C2/c$
a/Å	14.022(4)	17.206(6)
b/Å	7.417(2)	13.808(3)
c/Å	13.758(4)	13.936(4)
α/^{o}	90.00	90.00
β/^{o}	90.41(3)	122.01(3)
γ/^{o}	90.00	90.00
V/Å^3	1430.77(7)	2807.35(14)
Z	4	4
ρ_c/g cm^{-3}	1.329	1.820

μ /mm^{-1}	0.097	5.541
Reflections collected	5133	16304
Unique reflections	2810	2757
R_{int}	0.021	0.038
$R_1{}^a$ (I > 2σ(I))	0.036	0.018
$wR_2{}^b$ (all data)	0.099	0.042

[a] $R_1 = \sum||F_o|-|F_c||/\sum|F_o|$.

[b] $wR_2 = [\sum w(F_o^2-F_c^2)^2/\sum w(F_o^2)^2]^{1/2}$

Single crystals of **A4** were obtained by diffusion of EtOH to dichloromethane solution of **A4**. Single-crystal X-ray diffraction study reveals that **A4** crystallized in the monoclinic crystal system with $P2_1/c$ space group. The crystallographic details are provided in Table 2. A large planar can be seen between benzene and aminomalonitrile, which are quite conjugated as shown in Fig. 9a. The C–C and C–N bonds distances are in the range of 1.370(20)–1.458(19) and 1.285(18)–1.392(18) Å, respectively. There exists weak non-classical C–H···O intramolecular hydrogen bonds involving methoxy groups with methenyl group (C···O = 2.804–3.464 Å) as well as N–H···N intramolecular interaction between the amino and imino group (N···N = 2.791 Å), which play a vital role in the consolidation of the **A4** molecule. Via N–H···N intermolecular interactions between the amino and neighboring cyano groups (N···N = 3.020–3.088 Å, N–H···N = 137–169°) as well as the nonclassical C–H···O hydrogen bonds interaction between benzene rings and neighboring methoxy groups (C···O = 3.393 Å, C–H···O = 151°), the **A4** molecules are interlinked into a two-dimensional supramolecular network (Fig. 9c).

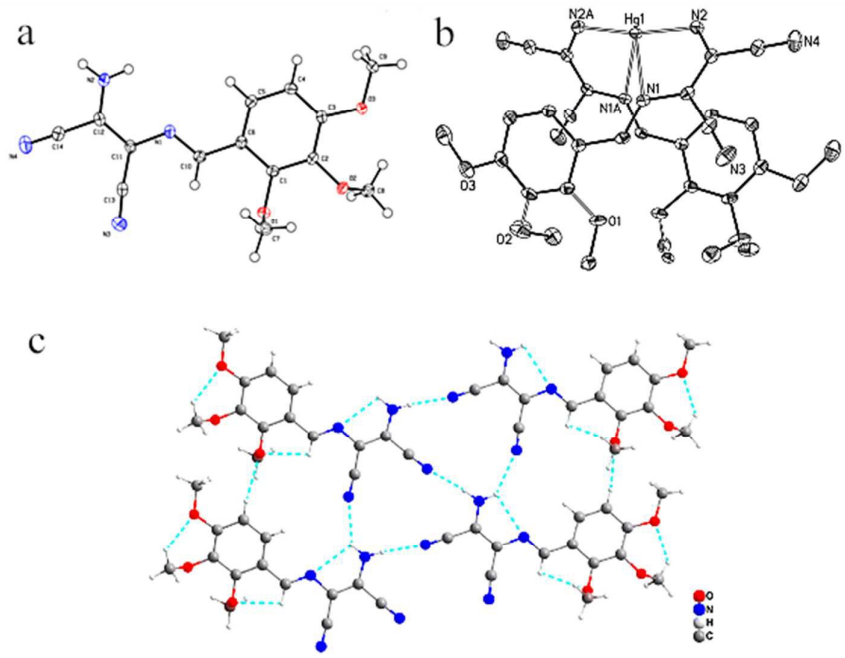

Fig. 9. (a) Molecular structure of **A4**. (b) Coordination structure of complex **B4**. H atoms omitted for clarity. (c) Perspective views of hydrogen-bonding interactions in **A4**.

It also reveals that complex **B4** crystallized in the monoclinic crystal system with *C*2/*c* space group. The asymmetric unit contains one half of the formula unit and consists of one crystallographically unique Hg atom and one **A4** (Fig. 9b). Hg atom lies in a special position (SOF = 0.5), being four-coordinated by two amino and two imino nitrogen atoms from two different **A4** (Hg–N = 2.034(2)–2.647(2) Å). The two **A4** molecules have a dihedral angle ca. 19.69° (based on the benzene rings), being located at the same side of Hg atom. There exists weak non-classical C–H···O intramolecular hydrogen bonds between methoxy groups (C···O = 2.826–3.168 Å), which play a significant role in the construction of the mononuclear Hg unit. Via C–H···N intermolecular interactions between the

methoxy groups and neighboring cyano groups (C···N = 3.106–3.457 Å, N–H···N = 102–149°), the **B4** molecules are interlinked into a two-dimensional supramolecular network (Fig. 10).

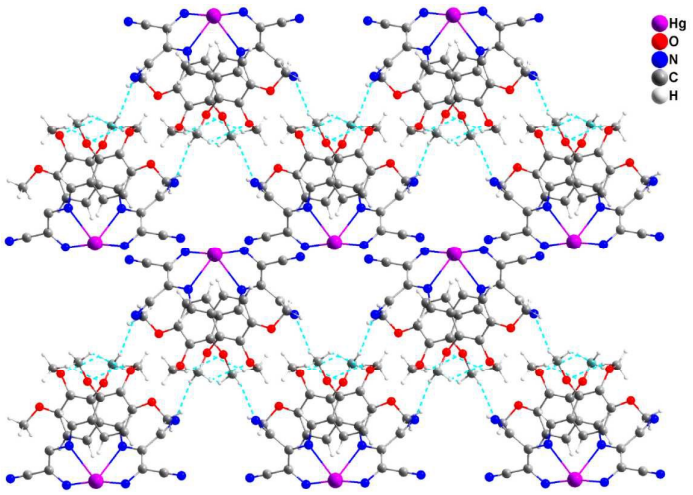

Fig.10. 2D supramolecular structure of **B4** mediated by hydrogen bonds

Theoretical calculation study

In order to further understand the behavior of **A4** with the Hg^{2+}, DFT calculations have been carried out. As Hg^{2+} is known for its four-coordination complex, the input structures were designed in the same way to have bidentate coordination with DMN. The structural optimization was done using the Gaussian 09W package adopting the B3LYP method with SDD as the basic set. TD-DFT calculations investigate the change of the absorption spectra upon addition of Hg^{2+}. Electron density of both HOMO and LUMO of **A4** and **B4** lies on the electron-withdrawing part. From the energy level diagram (Fig.12), it can be seen that addition of the metal ions leads to the stabilization of the HOMO and LUMO of these

chemosenors. Both HOMO and LUMO of the **B4** and **A4** were shown in Fig. 11, which are mainly dominated by molecular orbitals from **A4**. The contribution from Hg^{2+} ion to all these orbitals is significant. The electron density of the HOMO is localized on the whole conjugate part of the molecular, whereas the LUMO distribute on the diaminomaleonitrile and the imine moiety. For complex **B4**, its HOMO is more strongly localized than that in **A4**, and the localization on the cyano group of the diaminomaleonitrile from Hg atom is disappeared. The LUMO of complex **B4** is more located in the benzene ring and its localization on the cyano group of diaminomaleonitrile from Hg atom is also disappeared. Therefore, it can be concluded that the electronic π–π* transition in these complexes are localized on the 2-substituted diaminomaleonitrile ligands.

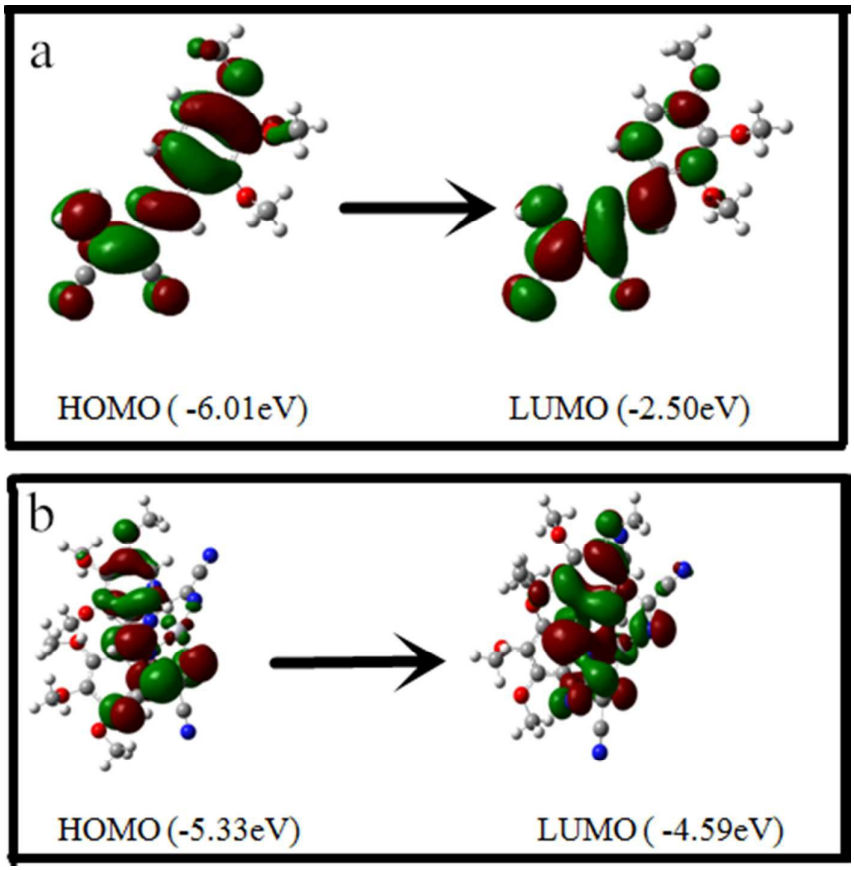

Fig. 11. HOMO and LUMO orbitals of **A4** (a) and **B4** (b) calculated on the DFT level.

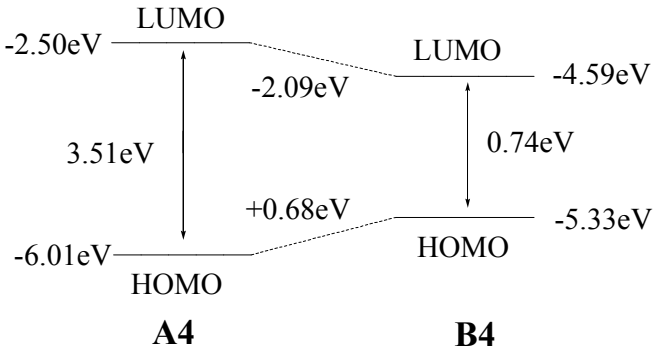

Fig. 12. Energy diagrams of HOMO and LUMO orbitals of **A4** and **B4** complex calculated on the DFT level.

The calculated HOMO–LUMO energy gaps (E_g) are summarized in Fig. 12. From the energy level diagram, complex **B4** has a lower LUMO energy level of -4.59 eV, while ligand **A4** has that of -2.50 eV. So it can be

concluded that the coordination of Hg stabilized the LUMO of the complex**.** The HOMO energy levels of **A4** and **B4** are calculated to be -6.01 and -5.33 eV, respectively, showing that the HOMO energy level of **A4** is a bit higher than that of **B4**. The calculated HOMO–LUMO energy gaps (E_g) obtained from DFT calculations were 3.51 and 0.74 eV for **A4** and **B4**, respectively. The complex **B4** has much smaller energy gap and longer wavelength of emission than that of **A4**. These data are consistent with the optical energy gaps as well as the band gap trend is in good agreement with the optical data.

Conclusion

In summary, five diaminomaleonitrile-based chemosensors were designed for naked-eye detection of Hg^{2+}, which were investigated with much higher selectivity over other competitive metal ions. They displayed strong colorimetric responses with slight red-shift absorptions that were useful for easy detection of Hg^{2+} by naked eyes visualization. Adequate characterization and studies were carried out to confirm the chemosensors **A1**–**A5** and their sensing behaviors toward Hg^{2+} ion. The binding mode study showed that the diaminomaleonitrile chemosensor formed a 2 : 1 complex with Hg^{2+} where the imine group played a critical role in the selective binding of Hg^{2+} ion. Their recognition behavior can function well over a wide range of pH value, making them suitable for detection of Hg^{2+} ion in industrial and environmental fields.

Acknowledgment

This work was supported by the National Natural Science Foundation of China (21172047 and 21372051), the Excellent Young Teacher Development Project of Universities in Guangdong Province (261532106) and the Guangzhou Science and Technology Program (201510010156).

Appendix A. Supplementary material

Crystallographic data for the structural analysis have been deposited with the Cambridge Crystallographic Data Centre. The CCDC number of **A4** and **B4** are 994864, 994865, respectively. Copies of this information can be obtained free of charge from The Director, CCDC, 12 Union Road, Cambridge, CB2 1EZ, UK (Tel: + 44(0)1223 762911. E-mail: deposit@ccdc.cam.ac.uk or www: http://www.ccdc.cam.ac.uk).

Notes and references

1 P. B. Tchounwou, W. K. Ayensu, N. Ninashvili, D. Sutton, Environ. Toxicol., 2003, **18**,149–175.

2 T. W. Clarkson, L. Magos, G. J. Myers, N. Engl. J. Med., 2003, **349**, 1731–1737.

3 Q. Zhao, F. Y. Li, C. H. Huang, Chem. Soc. Rev., 2010, **39**, 3007–3030.

4 Y. M. Yang, Q. Zhao, W. Feng, Chem. Rev., 2013, **113**, 192−270.

5 A. T. Wright, E. V. Anslyn, Chem. Soc. Rev., 2006, **35**, 14–28.

6 E. M. Nolan, S. J. Lippard,Chem. Rev., 2008, **108**, 3443–3480.

7 B. H. Tong, Y. Zhang, Z. Han, D. Y. Chen, Q. F. Zhang, Inorg. Chem. Commun., 2013, **28**, 31–36.

8 J. M. Lo, J. C. Yu, F. I. Hutchison, C. M. Wai, Anal. chem., 1982, **54**, 2536–2539.

9 H. N. Kim, W. X. Ren, J. S. Kim, J. Yoon, Chem. Soc. Rev., 2012, **41**, 3210–3244.

10 D. Sareen, P. Kaur and K. Singh, Coord. Chem. Rev., 2014, **265**, 125–154.

11 M. E. Jun, B. Roy and K. H. Ahn, Chem. Commun., 2011, **47**, 7583–7061.

12 X. Chen, T. Pradhan, F. Wang, J. S. Kim, J. Yoon, Chem. Rev., 2012, **112**, 1910–1956.

13 J. Jiang, W. Liu, J. Cheng, L. Yang, H. Jiang, D. Bai, W. Liu, Chem. Commun., 2012, **67**, 8371–8378.

14 J. Y. Park, B. G. In, L. N. Neupane, K. Lee, Analyst, 2015, **140**, 744–749.

15 Y. Yang, K. Yook, J. Tae, J. Am. Chem. Soc., 2005, **127**, 16760–16761.

16 J. Park, B. In, K. H. Lee, RSC Adv., 2015, **5**, 56356–56361.

17 S. H. Kim, S. Matsumoto, Dyes Pig., 2007, **72**, 406–408.

18 T. A. Schwarze, H. Kelling, M. Muller, T. Trautmann, O. Klamroth, P. S. Baumann, H. J. Holdt, Chem. Eur. J. 2012, **18**, 10506–10510.

29 G. Consiglio, S. Failla, P. Finocchiaro, I. P. Oliveri, R. Purrello, S. D. Bella, Inorg. Chem., 2010, **49**, 5134–5142.

20 V. Kumar, A. Kumar, U. Diwan, Shweta, Ramesh, S. K. Srivastava, K. K. Upadhyay, Sensors and Actuators B, 2015, **207**, 650–657.

21 X. B. Sun, Y. Q. Liu, X. J. Xu, G. Yu, S. Y. Chen, W. F. Qiu, Y. Q. Ma, Z. H. Zhao, D. B. Zhu, synthetic metals, 2006, **156**, 1174–1181.

22 L. Wang, P. Shen, Z. C. Cao, X. P. Liu, Y. S. Huang, C. Y. Liu, P. Chen, B. Zhao, S. T. Tan, J. Power Sources, 2014, **246**, 831–839.

23 M. J. Maclachlan, M. K. Park, L. K. Thompson, Inorg. Chem., 1996, **35**, 5492–5499.

24 S. Pagliari, R. Corradini, G. Galaverna, S. Sforza, et al. Chem. Eur. J. 2004, 10, 2749–2758.

25 W. Li, Y. Zhang, X. Gan, M. Yang, B. Mie, M. Fang, Q. Zhang, J. Yu, J. Wu, Y. Tian, H. Zhou, Sensors and Actuators B, 2015, **206**, 640–646.

26 J. Diego, M. M. Ramon, S. Felix, S. Juan, Tetrahedron Lett., 2004, **45**, 1257–1259.

27 D. Jiménez, R. Martínez-Máñez, F. Sancenón, J. V. Ros-Lis, J. Soto, Á. Benito, E. García-Breijo, Eur. J. Inorg. Chem. 2005, 2393–403.

28 H. P. Zhou, J. Q. Wang, Y. X. Chen, W. G. Xi, Z. Zheng, D. L. Xu, Y. L. Cao, G. Liu, W. J. Zhu, J. Y. Wu, Y. P. Tian, Dyes Pig., 2013, **98**, 1–10.

29 J. Li, Y. Wu, F. Song, G. Wei, Y. Cheng and C. Zhu, J. Mater. Chem., 2012, **22**, 478–482.

30 M. Shellaiah, Y. H. Wu, A. Singh, M. V. Raju, H. C. Lin, J. Mater. Chem. A, 2013, **1**, 1310–1318.

31 Q. Li, M. Peng, N. Li, J. Qin, Z. Li, Sensors and Actuators B, 2012, **173**, 580– 584.

32 S. P. Wu, K. J. Du, Y. M. Sung, Dalton Trans., 2010, **39**, 4363–4368.